ADVANCES IN ATMOSPHERIC SCIENCES, VOL. 21, NO. 6, 2004, 928–940

Vorticity Budget Investigation of a Simulated Long-Lived Mesoscale Vortex in South China

CHEN Min*[1] (陈 敏) and ZHENG Yongguang[2] (郑永光)

[1] *Institute of Urban Meteorology, Beijing* 100089

[2] *School of Physics, Peking University, Beijing* 100871

(Received 16 November 2003; revised 11 May 2004)

ABSTRACT

A vorticity budget investigation is performed using the output data from a numerical simulation of a typical MCV (mesoscale convectively generated votex) case in South China. Results suggest that the divergence caused by convection in the low troposphere is the main producer of positive vorticity, while vertical vorticity transferred by the tilting term from the horizontal vorticity compensates the upward output of cyclonic vorticity. Scale analyses of the vorticity equation suggest that the advection of planetary vorticity can be neglected owing to the low latitude, which is different from the larger scale systems in high latitude areas. In addition, the distribution of relative vorticity tendency on pressure level is not uniform. A vortex will move along the vector from the negative to the positive vorticity tendency region. The mechanism of the phenomenon—that nearly all of the convectively ascending region is located southward/southeastward of the vortex center—is also discussed. Convergence with regard to latent heat release would be in favor of the spin-up of meso-vortex, however, the horizontal vorticity caused by wind shear is tilted by vertical motion due to convection. Consequently, the negative and positive vorticity tendencies are located symmetrically about the convective center, which suggests that the vortex southward movement is dynamically driven by convection.

Key words: Vorticity Budget, mesoscale convectively generated votex, mesoscale convective system

1. Introduction

Vorticity budgets have been derived from the GATE (GARP Atlantic Tropical Experiment) dataset (Sui and Yanai, 1986), from composite African wave disturbances again from GATE (Stevens, 1979; Shapiro, 1978), or from composites of western Pacific disturbances (Reed and Johnson, 1974). Recently, similar vorticity budgets have also been derived from AMEX (Australian Monsoon Experiment) by Davidson (1995). And the one-dimensional barotropic non-divergence vorticity equation was used by Fang and Wu (1998) to study the effect of vorticity source and momentum source on the atmospheric circulation. The consistent feature in these studies is the examination of the apparent sink/source of cyclonic vorticity. Also, all the above studies deal with synoptic scale circulations. When investigating mesoscale vorties, the way of handling the vorticity budget is a little different (Yu et al., 1999; Zhang, 1992). As the friction and sub-grid effects can be neglected, the tendency of cyclonic vorticity is represented by the direct summation of all the forcing terms. Regardless of the scales of the investigated vortex, it should be noted that there are some features in common in all of the results of vorticity budgets. For instance, Davidson (1995) pointed out that from the results of vorticity budgets for the mean of the entire experimental period of AMEX, balance generally exists between the stretching and horizontal advection. In fact, this kind of balance can be found in other vorticity budget studies (Yu et al., 1999; Zheng et al., 1995). Therefore, one aim of the current study is to explore some intrinsic facts about vorticies revealed from the vorticity budget of a simulated mesoscale vortex.

A significant number of mesoscale convective systems (MCSs) exhibit an organized rotational circulation, often referred to as a "mesoscale convectively generated vortex" (hereafter MCV). MCVs sometimes develop into inertially stable, long-lasting features that

*E-mail: mchen@ium.cn

play a prominent role in convective organization within the later stage of the parent MCS. A growing body of tropical and midlatitude observations indicates that such circulations are frequently found in the low to mid-troposphere (above 1.5 km altitude) of MCS stratiform precipitation regions and exhibit a wide range of horizontal scales from 20 to 200 km and commensurate lifetimes ranging from a couple of hours to several days.

Heavy rainfall events often occur during the period, which is called the "pre-flooding season" from May to June of each year in South China; most of these are caused by MCSs. During the past decades, many investigations have been done to recognize the synoptic environment and physical mechanism of MCSs in South China (Zhou et al., 2003; Xiang and Jiang, 1995; Wang et al., 2000). However, the studies on their mesoscale and microscale details are quite limited. As a typical case of HUAMEX (Huanan and Taiwan Area Mesoscale Experiment), heavy rainstorms occurred at 14 surface stations in the Pearl River Delta, the Western River drainage area, and Yangjiang County during 23–24 May 1998. It is revealed from infrared satellite images that an MCS developing from a single cloud cluster is responsible for the rainstorm (Wang et al., 2001). Also, the cloud systems and observation data showed the existence and sustaining of a circulative vortex. Therefore, this case may provide a good opportunity for us to understand the features and mechanisms of MCSs and associated MCVs in South China.

The aims of the current study are (1) to explore the distribution of the relative vorticity's tendency inside a mesoscale vortex; (2) to examine the intrinsic reasons for certain common phenomenon of vorticity budgets; (3) to get some idea of the dynamical aspects of MCVs in low latitude areas in South China; (4) to examine the relationship between the vortex and convection. In section 2, we provide an overview of the current MCV event. A brief introduction to the numerical model and a verification of the results are given in section 3. A description of the analysis method of the vorticity budget is provided in section 4. Section 5 describes the results of the budget analysis. Some further discussions about the vorticity's generation are shown in section 6.

2. Overview of the MCV event

Some MCSs in South China may occur near the quasi-stationary front at 850 hPa, or at the place where the west end of the shear line merges with the north edge of the southwest monsoon (Fang, 1986; Xiang and Jiang, 1995). From the conventional surface and sounding observation data, the MCV of our interest was initiated in an environment with a strong cold front moving quickly fast towards South China. At about 1200 UTC 23 May 1998, convection was active over the north of the Leizhou Peninsula and began over the west of the Pearl River Delta (see Fig. 1b). During the subsequent hours, the convective system developed and grew in size. Until 0100 UTC 24 May, its cold cloud cover displayed a rounded shape with its TBB value below –70°C (see Fig. 1d). Thereafter, it split into several meso-β scale convective systems and began to dissipate (see Fig. 1f). Meanwhile, an inspection of the sounding observation data analyses at 850 hPa reveals that a meso-scale circulative vortex, which already formed before 1200 UTC 23 May, moved southeastward with the MCS from the west end of the shear line representing the cold front during the period from 1200 UTC 23 May to 1200 UTC 24 May 1998 (see Figs. 1a, 1c, and 1e). And no information about the vortex could be identified above 700 hPa (figures omitted). Therefore, the vortex just existed in low troposphere.

3. Model description and verification

3.1 *Model description*

The Pennsylvania State University-National Center for Atmospheric Research Fifth-generation Mesoscale Model (MM5), a nonhydrostatic, primitive-equation model (Grell et al., 1994), was employed. The simulation featured 26 unequally-spaced terrain-following-coordinate (σ) levels in the vertical. Here, $\sigma = (p - p_{\rm top})/(p_{\rm sfc} - p_{\rm top}), p$ is pressure, $p_{\rm top}$ is the pressure at the model top (100 hPa), and $p_{\rm sfc}$ is the surface pressure. Two nested domains with the center located at (23°N, 113°E) are shown in Fig. 2. The dimensions of the fine mesh and coarse mesh are $61 \times 85 \times 26$ and $41 \times 61 \times 26$, and their grid distances are 15 km and 45 km respectively. Precipitation processes were parameterized using an explicit-moisture scheme that includes prognostic equations for water vapor, cloud water, rain water, snow, graupel and ice crystals (Reisner et al., 1998). The Grell cumulus parameterization (Grell, 1993) was used to represent subgrid-scale convective precipitation. Other parameterizations included a multilevel planetary boundary layer (Zhang and Anthes, 1982) and a radiative scheme involving longwave and shortwave radiation (Dudhia, 1989). To create the initial conditions for the model simulation, an analysis from the data assimilation system of SCSMEX were interpolated to the model grid as the first guess. The conventional surface and sounding observation data were used to modify the first guess after being objectively analyzed. Lateral boundary conditions were generated by a linear inter-

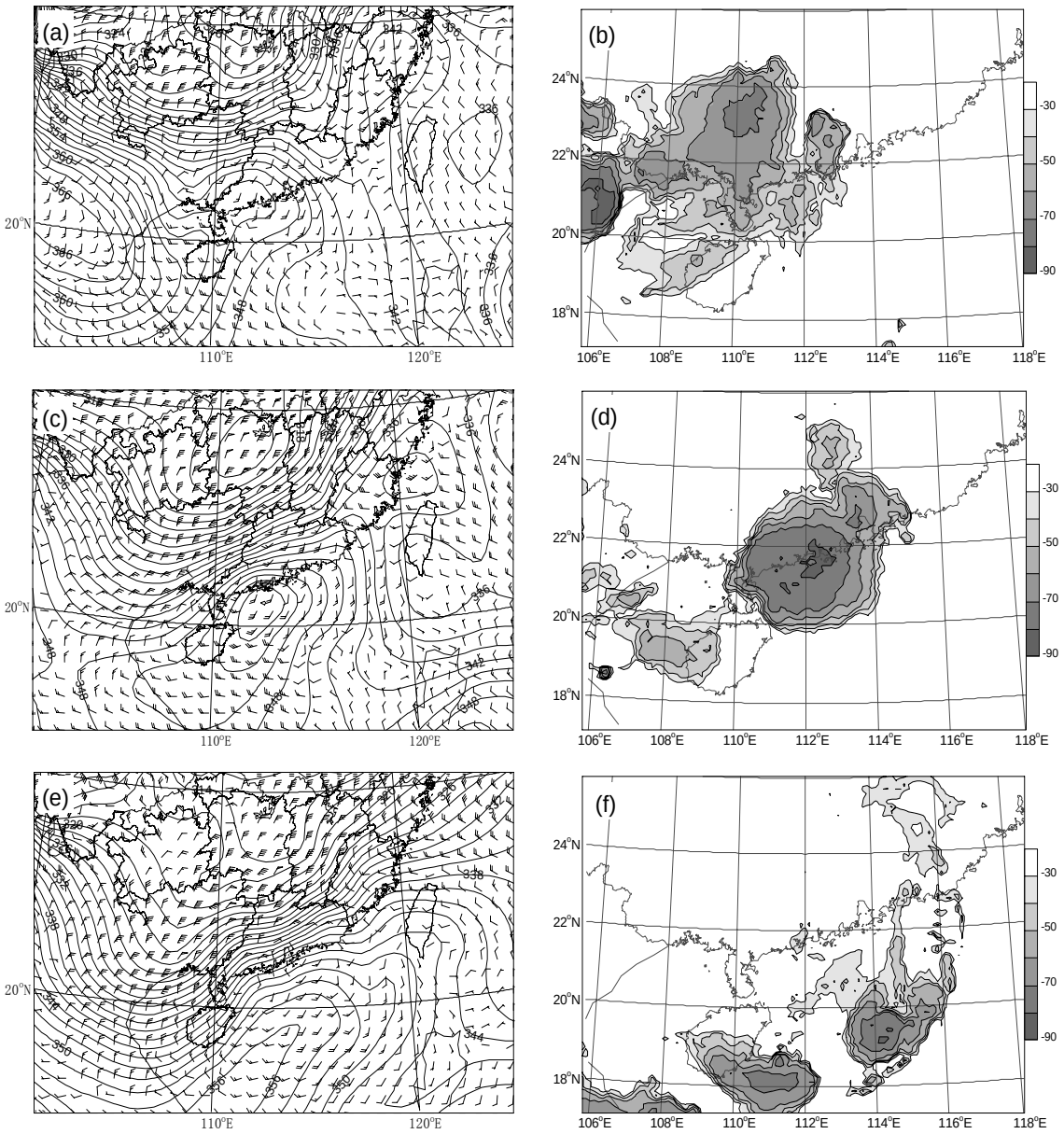

Fig. 1. Equivalent potential temperature and wind analysis at (a) 1200 UTC 23 May 1998, (c) 0000 UTC 24 May 1998, (e) 1200 UTC 24 May 1998, and TBB contours retrieved from infrared satellite images for (b) 1200 UTC 23 May 1998, (d) 0100 UTC 24 May 1998, (f) 1100 UTC 24 May 1998.

polation of the assimilated analyses at 6-h intervals.

The simulation was initialized at 0000 UTC 23 May 1998 and ended at 1200 UTC 24 May 1998. Such a period covers the main procedures of the formation, maturation, and dissipation of the MCS.

3.2 *Verification of results*

The 24-h (i.e., from 0000 UTC 23 May to 0000 UTC 24 May) forecast precipitation of the nested domain for this event is shown in Fig. 3b. Compared with the observation, the location of the main northwest-to-southeast oriented precipitation area may correspond to a series of small precipitation centers to the north of the Leizhou Pennisula. It reflects the path of the MCV and its associated MCS moving from Yunnan Province to the South China Sea. The other two main forecast precipitation centers, one located to the northwest of the Pearl River Delta and the other located in the south of Guangdong Province, are also quite similar with the observations.

As TBB (Temperature of Black Body) data retrieved from satellite images can be used as a criter-

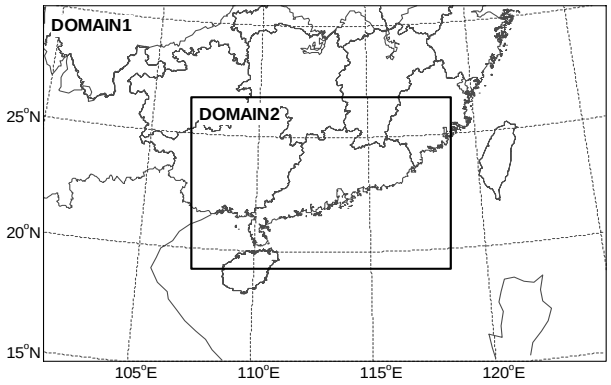

Fig. 2. The simulated domain area.

ion of MCS, the ice mix ratio output from the model can also be used to identify the simulated MCS. The contours of simulated ice mix-ratio from t=25–27 h (the corresponding time is from 0100 UTC 24 May to 0300 UTC 24 May) with a 1-h interval at 300 hPa are shown in Fig. 4. Obviously, the rounded cold cloud cover located to the northeast of Hainan Island at 0200 UTC 24 May 1998 was a typical feature of the MCC (see Fig. 4d), and it began to dissipate starting from 0300 UTC (see Fig. 4f). At the corresponding time in the simulation, the ICE mix-ratio contours at 300 hPa also displayed an MCS with a similar shape located to the west of the Pearl River Delta. The course of its development cannot be determined due to the lack of infrared images from 2200 UTC 23 May to 0000 UTC 24 May. However, the simulation may provide some useful clues about it. The above comparison suggests that the simulation was quite successful and credible, and it may provide a high-resolution, dynamically consistent dataset for us to analyze further.

4. Meso-scale vorticity budget

4.1 *Formulation*

As a common method to investigate the physical process about a vorticity's generation, the vorticity budget can be formulated by evaluating all the terms in the vorticity equation using the three-dimensional wind fields derived from the model's output. Ignoring friction and sub-grid effects, the vertical vorticity equation inferred from the horizontal momentum equations of MM5 can be written in pressure coordinates as

$$\left(\frac{\partial \zeta_p}{\partial t}\right)_p = -\left[u\left(\frac{\partial \zeta_p}{\partial x}\right)_p + v\left(\frac{\partial \zeta_p}{\partial y}\right)_p\right] - \omega\left(\frac{\partial \zeta_p}{\partial p}\right)_p - v\left(\frac{\partial f}{\partial y}\right)_p - (\zeta_p + f)\left[\left(\frac{\partial u}{\partial x}\right)_p + \left(\frac{\partial v}{\partial y}\right)_p\right] + \left[\left(\frac{\partial \omega}{\partial y}\right)_p \frac{\partial u}{\partial p} - \left(\frac{\partial \omega}{\partial x}\right)_p \frac{\partial v}{\partial p}\right], \quad (1)$$

where f is Coriolis parameter, and ζ is relative vorticity,

$$\zeta_p = \left(\frac{\partial v}{\partial x}\right)_p - \left(\frac{\partial u}{\partial y}\right)_p$$

is the vertical component of relative vorticity, u and v are the two horizontal components of wind, and $\omega = \partial p/\partial t$ is vertical velocity. The subscript p, which represents pressure coordinates, will be omitted in the following text for the sake of convenience. The tendency term is labeled $\zeta_{\rm ten}$ and it represents the local variation of relative vorticity. The five terms on the right side of Eq. (1) can be described as follows:

(1) $\zeta_{\rm hadv} = -\left(u\dfrac{\partial \zeta}{\partial x} + v\dfrac{\partial \zeta}{\partial y}\right)$ is the horizontal advection term. It is caused by the non-uniform horizontal distribution of relative vorticity,

(2) $\zeta_{\rm vadv} = -\omega\dfrac{\partial \zeta}{\partial p}$ is the convective term which denotes the vertical advection of relative vorticity due to vertical motion,

(3) $\zeta_{\rm fadv} = -v\dfrac{\partial f}{\partial y}$ is the advection term of planetary vorticity. It denotes the variation of relative vorticity due to the conservation of absolute vorticity when the air parcel moves longitudinally,

(4) $\zeta_{\rm div} = -(f+\zeta)\left(\dfrac{\partial u}{\partial x} + \dfrac{\partial v}{\partial y}\right)$ denotes the divergence (stretching) term, representing the amplification(reduction) of preexisting vertical vorticity by horizontal convergence (divergence),

(5) $\zeta_{\rm tilt} = -\left(\dfrac{\partial \omega}{\partial x}\dfrac{\partial v}{\partial p} - \dfrac{\partial \omega}{\partial y}\dfrac{\partial u}{\partial p}\right)$ is the tilting term, denoting the vertical vorticity created by the tilting of horizontal vorticity by horizontally non-uniform distributions of vertical motion.

Then, the local change of relative vorticity can be expressed as:

$$\zeta_{\rm ten} = \frac{\partial \zeta}{\partial t} = \zeta_{\rm hadv} + \zeta_{\rm vadv} + \zeta_{\rm fadv} + \zeta_{\rm div} + \zeta_{\rm tilt}$$

Using the output data of the simulation, the terms on the right-hand side of Eq. (1) can be determined at each grid point on the 23 vertical pressure levels from 1000–100 hPa. All terms' summation represents the magnitude of the local change of relative vorticity ($\zeta_{\rm ten}$) at each grid and a domain average of each term in the vortex area can be easily obtained after simple

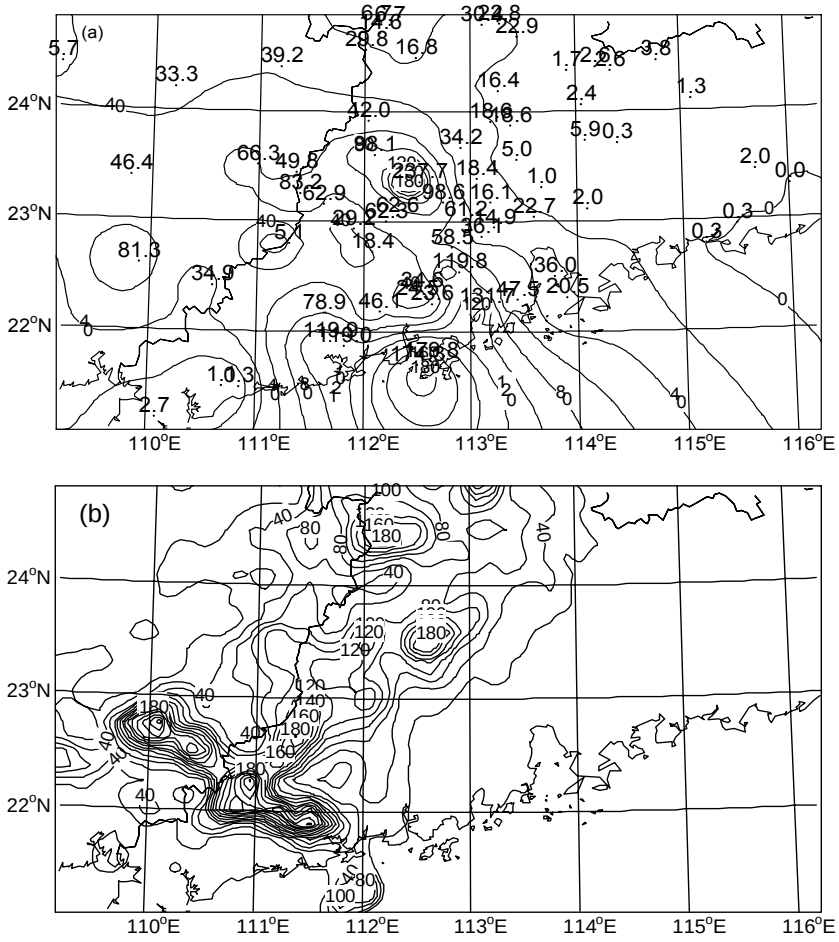

Fig. 3. (a) The observed total precipitation from 0000 UTC 23 May to 0000 UTC 24 May and (b) the 24-h (i.e., from 0000 UTC 23 May to 0000 UTC 24 May) forecast precipitation (units: mm) in the nested domain.

statistical calculation.

5. Budget analysis

To avoid the negative impact of the spin-up process of the simulation in the first 6 hours, we choose $t = 13$ h and $t = 24$ h, respectively, of the nested forecasts as the two typical moments of the vortex development and sustainment to investigate the vorticity budget (Fig. 5).

5.1 *Vortex development*

Figure 6a illustrates the distributions of the simulated wind field and relative vorticity tendency of the nested domain at 850 hPa at $t = 13$ h.The mean vertical structures of the terms in the budget equation are shown for the area c which covers the vortex at 850 hPa in Fig. 7a[1]. We note that below 600 hPa, the positive divergence term ($\zeta_{\rm div}$) and the negative advection term ($\zeta_{\rm hadv}$) are of similar magnitude. Meanwhile, a certain balance also exists above 600 hPa between the positive convective term ($\zeta_{\rm adv}$) and the negative tilting term ($\zeta_{\rm tilt}$). Consequently, the tendency term ($\zeta_{\rm ten}$) is quite weak throughout the whole troposphere. However, there is a pronounced couplet of a positive (negative) area of vorticity tendency located relative to the east (west) side of the circulation center (Fig. 6a and Fig. 6c). Perhaps the co-existence of the positive (negative) couplet leads to a weak tendency at 850 hPa when the area average is calculated. On the other hand, such an uneven distribution is considered as a certain mechanism that drives the vortex to move at a certain pressure level, i.e., the vertical vorticity would amplify (weaken) in area with positive (negative) tendency and sequentially the vortex would move following the track of relative vorticity amplification.

[1]The vertical profile of $\zeta_{\rm adv}$ is omitted here and the reason will be stated in the following parts.

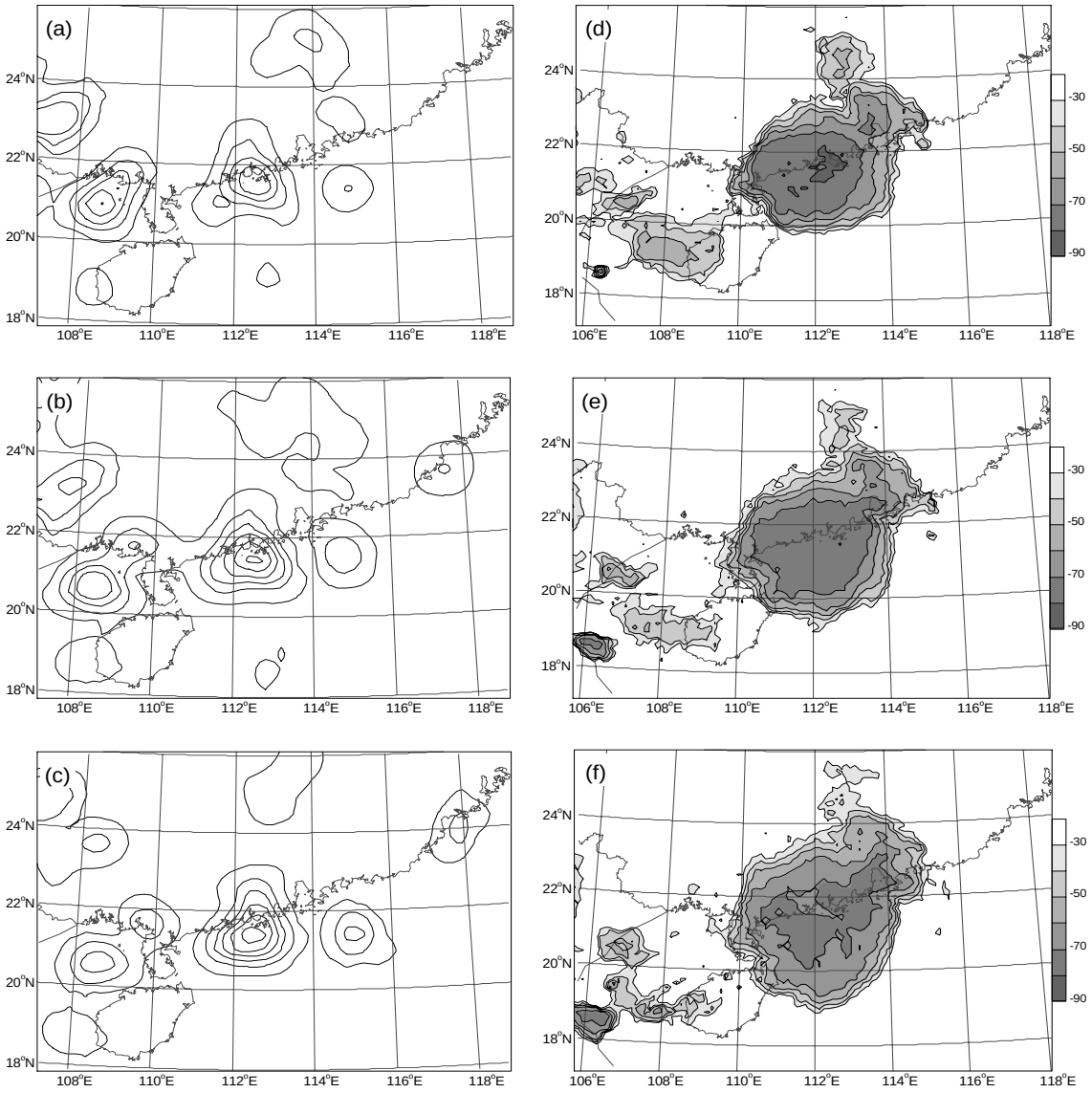

Fig. 4. The simulated ICE mix ratio at 300 hPa at (a) $t = 25$ h, (c) $t = 26$ h, (e) $t = 27$ h and TBB contours retrieved from infrared satellite images for (b) 0100 UTC,(d) 0200 UTC, (f) 0300 UTC 24 May 1998.

To obtain more knowledge about how positive vorticity tendency is produced, various terms of the relative vorticity equation are averaged in the domain d that mainly covers the positive area at 850 hPa (Fig. 6c). Figure 7b illustrates the vertical profiles of each item in the vorticity equation. Obviously, there is an intense positive tendency in the low to mid-troposphere under 400 hPa, among which the magnitude even reaches 10^{-7} s^{-2} below 850 hPa and from 600 hPa to 500 hPa. The stretching term caused by the intense convergence southeastward of the vortex is the main producer of the positive tendency in the low troposphere, especially below 700 hPa. Above 700 hPa, the vorticity's transportation by updraft makes the convection term a major positive contributor. In the boundary layer below 900 hPa, the tilting term produces some positive vorticity that is restrained by the negative convective term, i.e., in the low troposphere, the vertical vorticity transferred by the tilting term from the horizontal vorticity compensates the upward output of the cyclonic vorticity. In conclusion, according to the vertical profile of the four main contributors of the vorticity budget (Fig. 7a and Fig. 7b), the two terms (divergence and advection) related to horizontal motion may mostly affect the vorticity budget in the low troposphere, while the other two terms

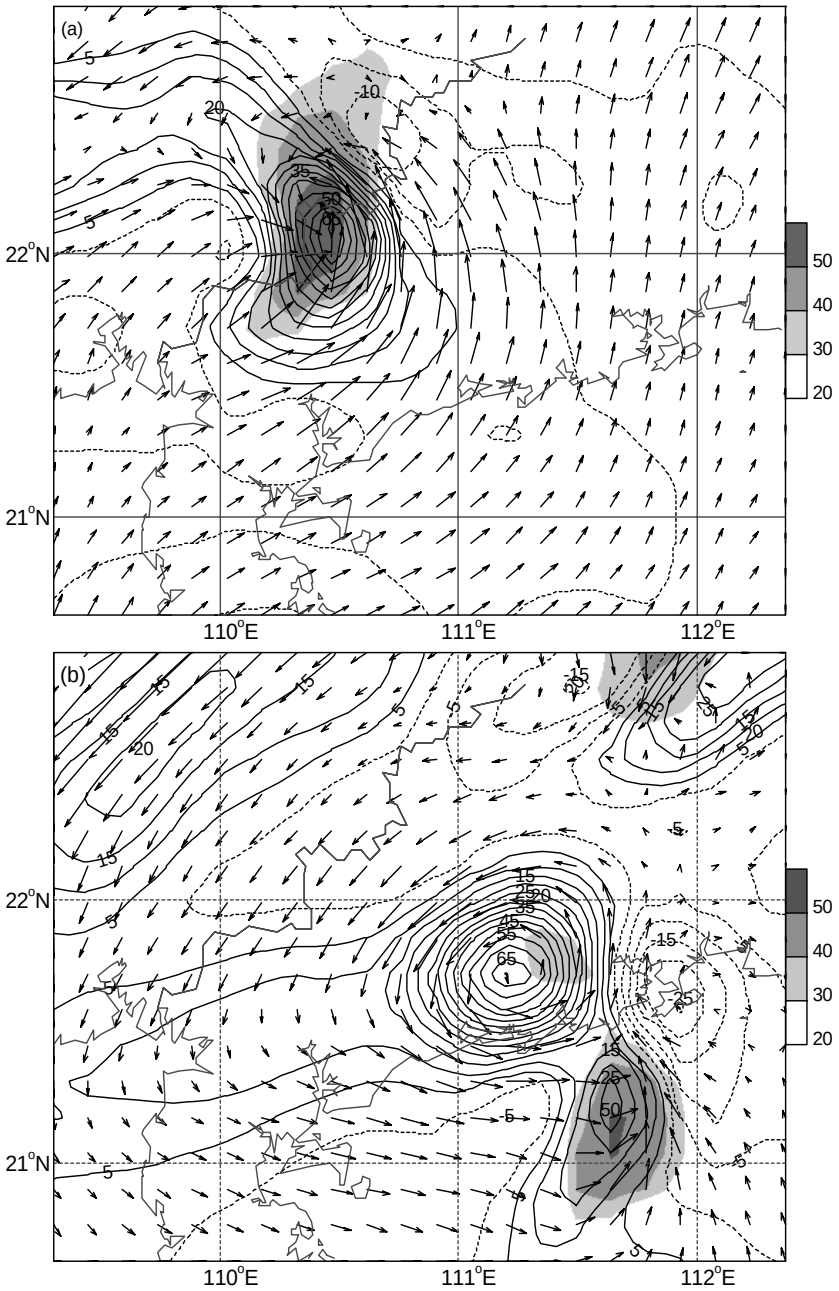

Fig. 5. Distributions of relative vorticity (solid line; units: 10^{-6} s^{-1}; dashed lines are negative.) at 850 hPa at (a) $t = 13$ h and (b) $t = 24$ h. The shaded area is where the simulated reflectivity is > 30 dBZ.

(convection and tilting) caused by the vertical motion may mostly influence the vorticity status in the mid-troposphere. Furthermore, the trends of the effects of both couples are approximately opposite to each other.

Is such a balance between the divergence term and advection term case dependent or does it have some intrinsic reason? In view of the physical interpretation, the counteraction is not accidental. For instance, the relative vorticity ς is positive when the wind field is rotating cyclonically. If an air parcel is converging toward the vorticity center, the stretching term

$$-(f+\zeta)\left(\frac{\partial u}{\partial x}+\frac{\partial v}{\partial y}\right)>0\,.$$

Meanwhile, the air parcel is moving from the vorticity's low area toward the high area, so the advective

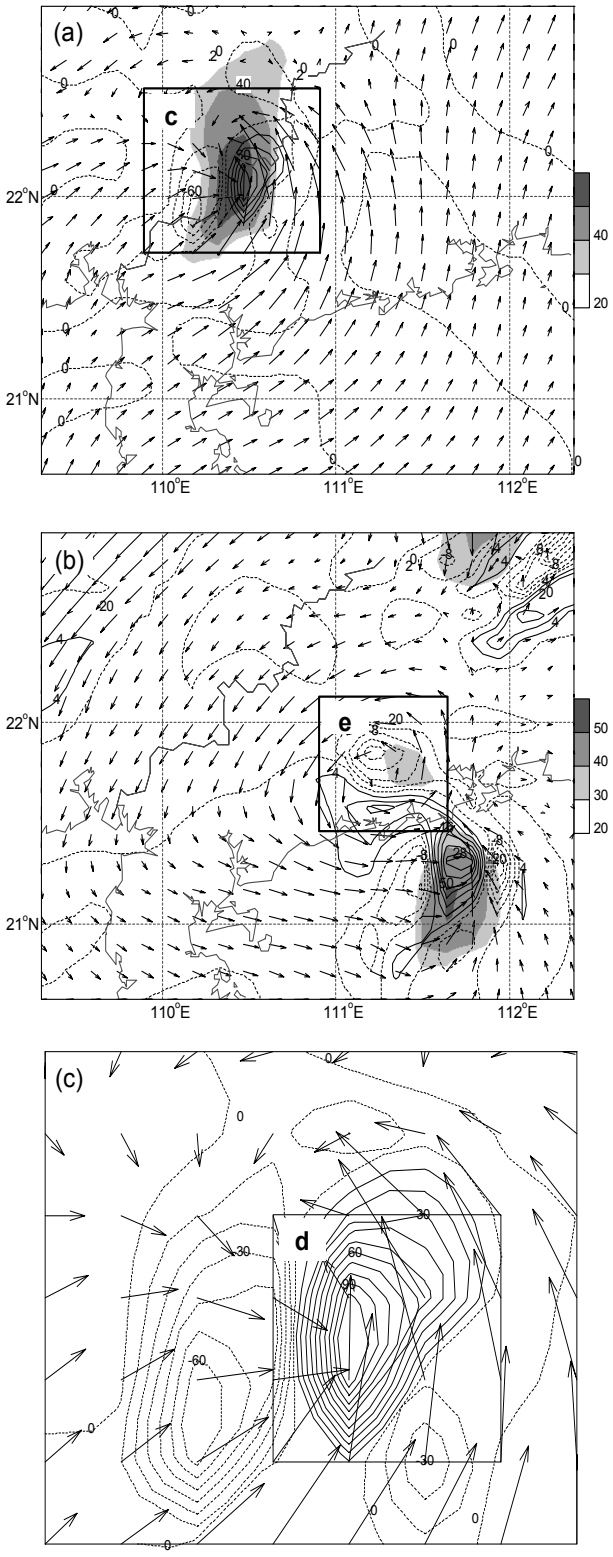

Fig. 6. Distributions of wind field and $\zeta_{\rm ten}$ (solid line represents $\zeta_{\rm ten} > 0$, dashed line represents $\zeta_{\rm ten} < 0$; units: 10^{-8} s^{-2}) at 850 hPa at (a), (c) $t = 13$ h, and (b) $t = 24$ h. The shaded area is where reflectivity is > 30 dBZ.

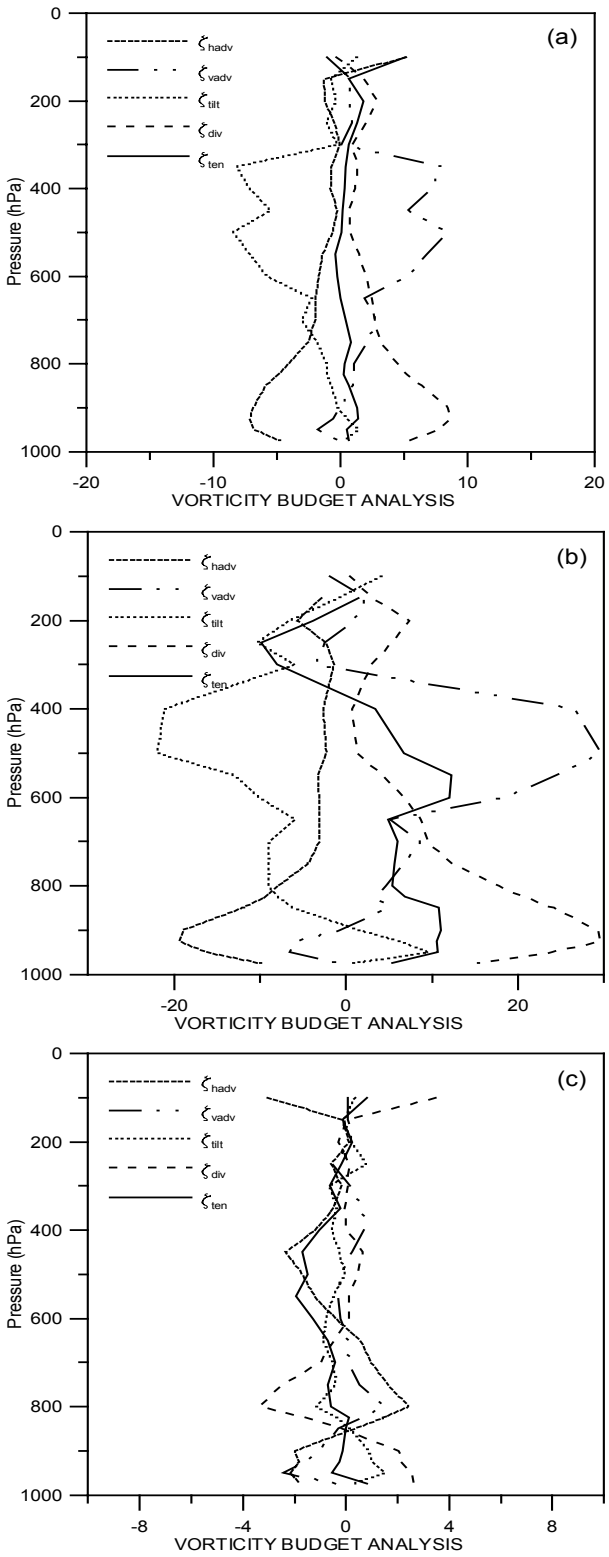

Fig. 7. The vertical profiles of various terms of the vorticity budget (units: 10^{-8} s^{-2}) of (a) domain c averaged at $t = 13$ h, (b) domain d averaged at $t = 13$ h, (c) domain e averaged at $t = 24$ h.

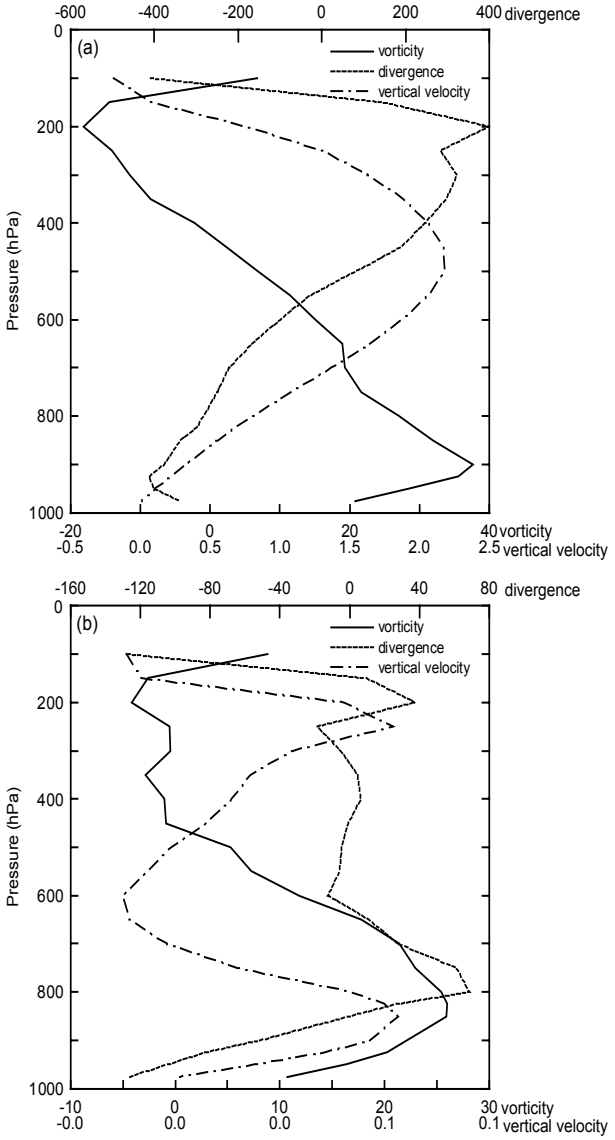

Fig. 8. Vertical profiles of the divergence(units: 10^{-6} s^{-1}), relative vorticity (units: 10^{-5} s^{-1}) and vertical velocity (units: m s^{-1}) (a) averaged in domain d at $t = 13$ h, (b) averaged in domain e at $t = 24$ h.

term

$$-\left(u\frac{\partial\zeta}{\partial x}+v\frac{\partial\zeta}{\partial y}\right)<0\,.$$

Similarly considering all the different configurations of vorticity and divergence, such counteraction is inevitable.

The average vertical profiles of the divergence, relative vorticity, and vertical velocity of domain are shown in Fig. 8. The maximum of the mean vertical velocity at 500 hPa (Fig. 8a) corresponds to the peak value of the convective term ($\zeta_{\rm adv}$) in the mid- troposphere (Fig. 7b). This indicates that the upward transportation of relative vorticity from low levels will enhance the tendency of cyclonic vorticity in the mid troposphere, especially during the developing stage of the vortex.

5.2 *Vortex sustainment*

Here we investigate the results at $t = 24$ h representing the sustaining stage of a vortex. At this time, the vortex is located northeastward of the Leizhou Peninsula. Convection is weakened remarkably inside the vortex as the simulated 30 dBZ convective echo just exists below 700 hPa. Simultaneously, new convective activity develops southeastward of the vortex.

Various terms of the vorticity equation at each level are averaged in a 90 km×90 km domain (as shown in Fig. 6b, domain e), which covers the closed cyclonic circulations at 850 hPa. The results of the vorticity budget are somewhat different from $t = 13$ h. Its net vorticity tendency is negative nearly throughout the whole troposphere (Fig. 7c). The stretching term's positive contribution prevails below 850 hPa, and its magnitude is less than one third of that at $t = 13$ h. Particularly, this term produces a negative tendency between 850 hPa and 600 hPa. The advection term's contribution is also opposite to that at $t = 13$ h. As the magnitude of the positive advection term is less than that of the negative divergence term, the net vorticity tendency is negative in the low troposphere.

The domain averaged upward motion (see Fig. 8b) is very weak at this time. That is why the tilting term and convective term do not play key roles in dominating the relative vorticity tendency as in the developing stage. Although a closed cyclonic circulation can be analyzed in the low troposphere, the flow field is evidently divergent (Fig. 8b), and that is why, at this time, the stretching term is negative.

6. Discussion

6.1 *Scale analyses of the vorticity equation*

Scale analysis is a common method when investigating dynamic problems. As this case took place in a low latitude area and since the researched vortex was a meso scale system, scales of each term on the right-hand side of the vorticity equation and their relative importance to the tendency would be different from the larger systems occurring in mid-high latitude areas.

Considering the actual magnitude of the simulation in the low troposphere of the low-latitude area, we set $U = 10$ m s^{-1}, $L = 10^5$ m, $\tau = L/U = 10^4$ s, $f_0 = 10^{-5}$ s^{-1}, $H = 10^4$ m, $p = 10$ hPa, $\Omega_0 = 10^{-1}$ Pa s^{-1} as characteristic scales of each conventional variable. Based on the results of the scale analysis on the horizontal motion equations documented in Atmosphere

Dynamics (Liu and Liu, 1991), the horizontal divergence is of the same scale as the vertical vorticity in low latitudse in view of the latent heat release, thus here, $\zeta_0 = D_0 = 10^{-4}\ \mathrm{s}^{-1}$.

The scale magnitude of each term in the vorticity equation can be estimated as

$$\zeta_{\mathrm{hadv}} = -\left(u\frac{\partial\zeta}{\partial x} + v\frac{\partial\zeta}{\partial y}\right) \sim 10^{-8}\ \mathrm{s}^{-2}\ ,$$

$$\zeta_{\mathrm{vadv}} = -\omega\frac{\partial\zeta}{\partial p} \sim 10^{-8}\ \mathrm{s}^{-2}\ ,$$

$$\zeta_{\mathrm{fadv}} = -v\frac{\partial f}{\partial y} \sim 10^{-9}\ \mathrm{s}^{-2}\ ,$$

$$\zeta_{\mathrm{div}} = -(f+\zeta)\left(\frac{\partial u}{\partial x} + \frac{\partial v}{\partial y}\right) \sim 10^{-8}\ \mathrm{s}^{-2}\ ,$$

$$\zeta_{\mathrm{tilt}} = -\left(\frac{\partial\omega}{\partial x}\frac{\partial v}{\partial p} - \frac{\partial\omega}{\partial y}\frac{\partial u}{\partial p}\right) \sim 10^{-8}\ \mathrm{s}^{-2}\ ,$$

$$\zeta_{\mathrm{ten}} = \frac{\partial\zeta}{\partial t} \sim 10^{-8}\ \mathrm{s}^{-2}$$

Obviously, the advection term of planetary vorticity (ζ_{fadv}) caused by the air parcel's longitudinal movement is one order of magnitude less than the other terms, (we have omitted its contribution to vorticity tendency when discussing the averaged profiles) which differs from the results of the scale analysis on synoptic systems (Luo, 1994; Duan et al., 2004). The scales of the other forcing terms are of the same magnitude. From this point of view, they are equal, main contributors to the vorticity tendency, and none of them is a dominating factor in the vorticity's local change. As a matter of fact, it can be found from the domain average results of the vorticity budget that the convective and tilting term, advection and stretching term are of similar magnitude and converse sign, i.e., their effects nearly balance each other. The fact that the scale magnitude of the vorticity tendency (ζ_{ten}) is the same as the other forcing terms also suggests such a balance.

6.2 *Rossby radius of deformation*

It has been recognized in previous theoretical and modeling studies that the absolute geometric size (or horizontal scale) of an atmospheric disturbance is not necessarily representative of its actual tendency with regard to geostrophic adjustment (Ooyama, 1982; Frank, 1983). Rather, this tendency is dependent on the ratio of the disturbance's representative horizontal scale to the Rossby radius of deformation (hereafter, R_{d}) corresponding to conditions within its environment. An important application of the Rossby radius of deformation is to identify the scale at which the rotational influence or the inertial stability of a system becomes important (Cotton and Anthes, 1989). The mathematical definition of R_{d} is given as

$$R_{\mathrm{d}} = NH/(\zeta+f)^{1/2}(2V_{\mathrm{T}}R^{-1}+f)^{1/2}\ , \qquad (2)$$

where N is the Brunt-Väisälä frequency,

$$N \equiv \left[\frac{g}{\theta}\left(\frac{\partial\theta}{\partial z}\right)\right]^{1/2}\ ,$$

H is the scale height of the disturbance, ζ is the vertical component of relative vorticity, f is the Coriolis parameter, V_{T} is the tangential component of wind, and R is the radius of curvature of the rotational flow. Essentially, R_{d} represents the ratio of vertical static stability and horizontal inertial stability. When a circulation has a horizontal scale greater than or nearly equal to R_{d}, then the pressure (i.e., mass) field dominates the evolution of the flow and the horizontal momentum tends to adjust to the imposed pressure field within the disturbance. The circulation thus achieves a quasi-balanced condition and is expected to be long lasting. Such circulations are sometimes said to be "dynamically large". Conversely, if the horizontal scale of the circulation is much smaller than R_{d}, the wind field will be dispersed rapidly away from the circulation by gravity waves. In this situation, the system of circulation is "dynamically small" and is in general short-lived.

In the current study with intense convection, latent heat release should be under consideration. The Brunt-Väisälä frequency in a saturated situation was revised by Durran and Klemp (1982) as

$$N_{\mathrm{m}}^2 = \frac{g}{1+q_{\mathrm{w}}}\left(\frac{\Gamma_{\mathrm{m}}}{\Gamma_{\mathrm{d}}}\frac{d\ln\theta_{\mathrm{q}}}{dz} - \frac{dq_{\mathrm{w}}}{dz}\right)\ ,$$

$$\theta_{\mathrm{q}} = \theta_e\left(\frac{T}{T_0}\right)^{c_{\mathrm{w}}q_{\mathrm{w}}}/c_{\mathrm{p}}$$

where Γ_{m} and Γ_{d} are the saturated and dry lapse rates, q_{w} the total water mixing ratio of the substance $q_{\mathrm{w}} = (q_{\mathrm{c}} + q_{\mathrm{r}} + q_{\mathrm{s}}); q_{\mathrm{c}}, q_{\mathrm{r}}$ and q_{s} are the cloud water rain water, and snow mixing ration respectively. c_{p} the specific heat at constant pressure of dry air, c_{w} the specific heat of liquid water. The remaining variables have conventional meanings. All of the thermodynamic parameters in the N_{m}^2 expression can be obtained from the output of the simulation.

The Rossby radius of deformation of the circulation on 850 hPa at $t = 13$ h are calculated. The saturated Brunt-Väisälä frequency with values from sounding of vortex's center is $N_{\mathrm{m}} = 4.53\times10^{-3}\ \mathrm{s}^{-1}$, and the corresponding adjustment time is nearly 3.7 minutes. H is set to be 3700 m as the vortex stretched upward from surface to 650 hPa. The average vertical vorticity in the vortex area on 850 hPa is $13.16\times10^{-5}\ \mathrm{s}^{-1}$ and the Coriolis parameter is $6.296\times10^{-5}\ \mathrm{s}^{-1}$. Average tangential wind V_{T} is set as $5\ \mathrm{m\ s}^{-1}$. The curvature radius of vortex is taken to be 30 km (cf., Fig. 1). With

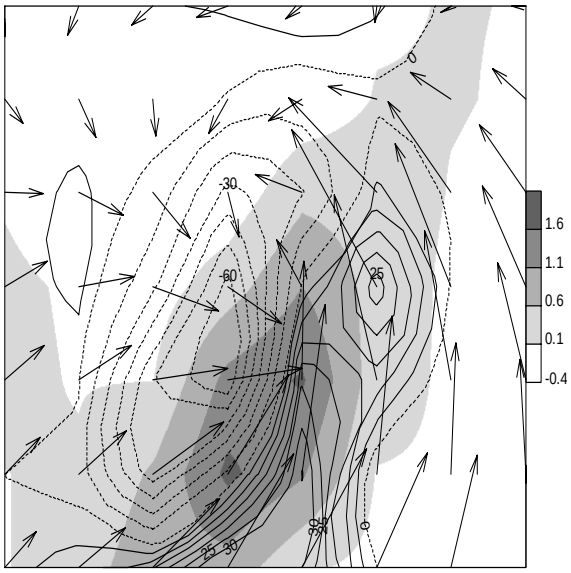

Fig. 9. In domain c, the horizontal distribution of the wind field, $\zeta_{\rm tilt}$ (solid line represents $\zeta_{\rm tilt} > 0$, dashed line represents $\zeta_{\rm tilt} < 0$, units: 10^{-8} s^{-2}) and vertical motion (shaded area, units: m s^{-1}) at 850 hPa at $t = 13$ h.

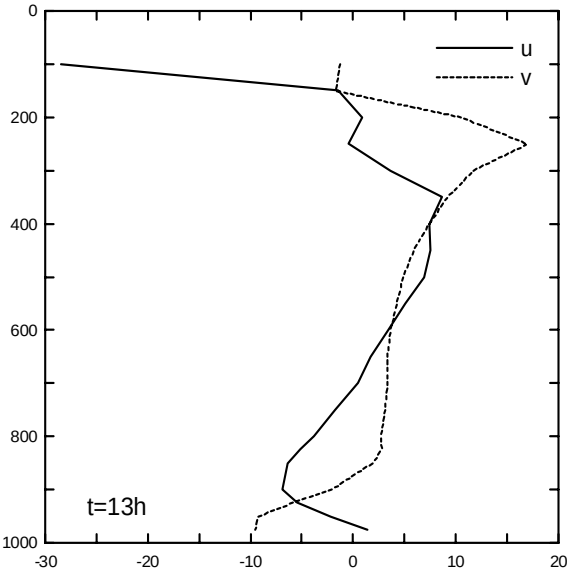

Fig. 10. Vertical profiles of averaged u (solid line, units: m s^{-1}) and v (dashed line, units: m s^{-1}) of the vortex center in domain c at 850 hPa at $t = 13$ h.

these values R_d is calculated to be 64 km. And it is very similar as 60 km, the scale of developing vortex's circulation at $t = 13$ h. Therefore, the vortex is "dynamically large", and it would last for a long time.

6.3 *Mechanism of meso-vortex sustainment in convection*

In this case, the developing process of the meso-vortex goes along with the evolution of deep convection. And nearly all of the convectively ascending region is located southward/southeastward of the vortex center.

The budget results, that the stretching and convective terms are the main positive contributors of vorticity tendency in the developing stage of the vortex, can be physically interpreted in terms of convection. Latent heat release caused by convection causes the air column to the stretched, so the pressure is depressed in the low troposphere and heightened in the high troposphere. The convergent flow in the low troposphere is driven to rotate by the Coriolis force, and leads to the amplification of the local vorticity tendency. This is identical with previous investigations that convergence with regard to latent heat release is in favor of the spin-up of the meso-vortex in MCC (Zhang and Fristch, 1987; Menard and Fristch, 1989).

The tilting term related with deep convection has been mentioned often. In many observation studies on meso-vortices, the tilting of horizontal vorticity by convective updrafts is thought to play a significant role in formation of the vortices (Verlinde and Cotton, 1990; Yu et al., 1999). Nevertheless, in the present case, the tilting of horizontal vorticity restrained the vortex in the northern end of convection. In Fig. 9 the couplet of the positive/negative tilting region at 850 hPa is distributed almost symmetrically about the updraft center. As a consequence, the vertical vorticity tendency also exhibits a distribution of a positive/negative couplet (cf., Fig. 6c).

Figure 10 gives the vertical profiles of the wind's two horizontal components at the vortex center at 850 hPa. u and v increase with altitude, i.e., $\partial u/\partial p < 0$ and $\partial v/\partial p < 0$. Owing to the place of this point relative to the updraft region, we have $\partial\omega/\partial x < 0$ and $\partial\omega/\partial y > 0$. Then

$$\zeta_{\rm tilt} = -\left(\frac{\partial\omega}{\partial x}\frac{\partial v}{\partial p} - \frac{\partial\omega}{\partial y}\frac{\partial u}{\partial p}\right) < 0\,,$$

i.e., to the north of the convective region, the tilting term is responsible for the reduction of vertical vorticity tendency inside the vortex.

The mechanism described by Weisman and Davis (1998) to explain a line-end vortex pair may be available to interpret this kind of symmetry. As the schematic of vertical vorticity generation through vortex tilting (Fig. 11) shows, for westerly shear, descending motion pushes the vortex line down in the center, resulting in cyclonic rotation on the north end and anticyclonic rotation on the south end. Localized ascent in the easterly shear produces the same vertical vorticity pattern.

In the current study, the situation is quite similar to the schematic. The wind shear described by Fig. 10 generates a northwest-southeast oriented horizontal

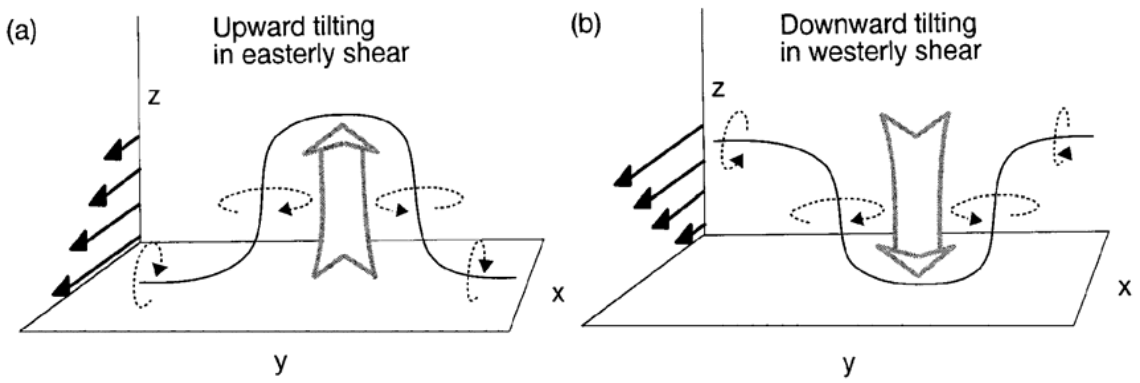

Fig. 11. The schematic of vertical vorticity generation through vortex tilting (Weisman and Davis, 1998).

vorticity. When the convection located to the southeast side of the vortex develops, the horizontal vortex line is tilted to generate anticyclonic vorticity on the northwest side and cyclonic vorticity on the southeast side of convection. In this way, the convection in current case will not enhance the vortex on its north end, whereas the cyclonic vorticity south of the convective region is amplified. From this point, the vortex's movement is caused by the vertical vorticity amplification on the convective region's southeast side and lessening to its northwest, which leads to an uneven distribution of the vorticity's tendency. Accordingly, the occurrence of convection located to the south of the vortex is dynamically responsible for the vortex moving southeastward.

7. Conclusions

Exploiting the export data of a numerical simulation, the domain-averaged vorticity budget is calculated. The results demonstrate that at the vortex's developing stage, the stretching term and convective term are the contributors of positive tendency in the low and middle troposphere respectively. The advection term and tilting term are the contributors of negative tendency. The real tendency is the net result of their counteraction. However, at the sustaining stage, the advection term generates positive tendency in the low level, while the stretching term is negative. The convective and tilting terms related to the vertical motion contribute much less than in the developing stage.

Scale analyses of the vorticity equation suggest that for a meso-vortex in low-latitude areas, the advection of planetary vorticity can be neglected owing to the low latitude. And the other forcing items' contributions to the vorticity tendency are of equal importance among themselves. The result is different from the larger scale systems in high latitude areas.

The mechanism of the phenomenon that nearly all of the convectively ascending region is located southward/southeastward of the vortex center is also discussed. Convergence with regard to latent heat release is favorable to the spinup of the meso-vortex. However, the horizontal vorticity caused by wind shear is tilted by vertical motion due to convection. As a consequence, negative and positive vorticity tendency are located symmetrically about the convective center. One may suppose that the vortex southward movement was dynamically driven by convection.

Acknowledgments. This research work was partly financially surpported by Beijing Municipal Science and Technology Commission under Cnontract H020620250330.

REFERENCES

Cotton，W. R., and R. A. Anthes，1989: *Storm and Cloud Dynamics*. Academic Press, 833pp.

Davidson, N. E., 1995: Vorticity budget for AMEX. Part I: Diagnostics. *Mon. Wea. Rev.*, **123**(6), 1620–1635.

Duan Yihong, Wu Rongsheng, Yu Hui, Liang Xudong, and Johnny C-L Chan, 2004: The Role of β-effect and a uniform current on tropical cyclone intensity. *Adv. Atmos. Sci.*, **21**(1), 75–86.

Dudhia, J., 1989: Numerical study of convection observed during winter monsoon experiment using a mesoscale two-dimensional model. *J. Atmos. Sci.*, **46**, 3077–3107.

Durren, D. R., and J. B. Klemp, 1982: On the effects of moistures on the Brunt-Välsälä frequency. *J. Atmos. Sci.*, **39**, 2152–2158.

Fang Juan, and Wu Rongsheng, 1998: Influences of vorticity source and momentum source on atmospheric circulation. *Adv. Atmos. Sci.*, **15**(1), 41–46.

Fang Zongyi, 1986: The preliminary study of medium-scale cloud clusters on changjiang basin in summer. *Adv. Atmos. Phys.*, **2**(3), 334–340.

Frank, W. M., 1983: The cumulus parameterization problem. *Mon. Wea. Rev.*, **111**, 1859–1871.

Grell, G. A., J. Dudhia, and D. R. Stauffer, 1994: A description of the fifth generation Penn State/NCAR Mesoscale model (MM5). NCAR Tech. Note, NCAR/TN-398+STR, 138pp.

Grell, G. A., 1993: Prognostic evaluation of assumptions used by cumulus parameterizations. *Mon. Wea. Rev.*, **121**, 746–787.

Liu Shikuo, and Liu Shida, 1991: *Atmospheric Dynamics*. Peking University Press, 269pp. (in Chinese)

Luo Zhexian, 1994: Study of effects of beta term and nonlinear advection on the structure of tropical cyclones. *Adv. Atmos. Sci.*, **11**, 391–398.

Menard, R. D., and J. M. Fritsich, 1989: A mesoscale convective complex-generated inertially stable warm core vortex. *Mon. Wea. Rev.*, **117**, 1237–1261.

Ooyama, K., 1982: Conceptual evolution of the theory and modeling of the tropical cyclone. *J. Meteor. Soc. Japan*, **60**, 369–379.

Reed, R. J., and R. H. Johnson, 1974: Vorticity budget of synoptic scale wave disturbances in the tropical western Pacific. *J. Atmos. Sci.*, **31**, 1784–1790.

Reisner, J., R. J. Rasmussen, and R. T. Bruintjes, 1998: Explicit forecasting of supercooled liquid water in winter storms using the MM5 mesoscale model. *Quart. J. Roy. Meteor. Soc.*, **124B**, 1071–1107.

Shapiro, L. J., 1978: Vorticity budget of a composite African wave disturbance. *Mon. Wea. Rev.*, **106**, 806–817.

Stevens, D. E., 1979: Vorticity, momentum and divergence budgets of synoptic-scale wave disturbances in the tropical eastern Atlantic. *Mon. Wea. Rev.*, **107**, 535–550.

Sui, C. H., and M. Yanai, 1986: Cumulus ensemble effects on the large-scale vorticity and momentum field of GATE. Part I. Observational evidence. *J. Atmos. Sci.*, **43**, 1618–1642.

Verlinde, J., and W. R. Cotton, 1990: A mesoscale vortex couplet observed in the trailing anvil of a multicellular convective complex. *Mon. Wea. Rev.*, **118**, 993–1010.

Wang Likun, Zheng Yongguang, Wang Hongqing, and Tao Zuyu, 2001: Preliminary analysis of environment and cloud clusters during Huanan Rainstorm Experiment. *Acta Meteorologica Sinica*, **59**(1), 115–119. (in Chinese)

Wang Yongming, Su Baixing, and Chao Yue, 2000: Cooperation of the system and feature of the circulation from South China Rainstorm Trial in 1998. *Jounal of Tropical Meteorology*, **16**(2), 123–130. (in Chinese)

Weisman, M. L., and Christopher A. Davis, 1998: Mechanisms for the generation of mesoscale vortices within quasi-linear convective systems. *J. Atmos. Sci.*, **55**(16), 2603–2622.

Xiang Xukang, and Jiang Jixi, 1995: Mesoscale convective complexes over the southern China Mainland. *Quarterly Journal of Applied Meteorology*, **6**(1), 9–17. (in Chineses)

Yu, C.-K., B. J.-D Jou, and F. Smull, 1999: Formative stage of a long-lived mesoscale vortex observed by airborne Doppler radar. *Mon. Wea. Rev.*, **127**(5), 838–857.

Zhang, D.-L., 1992: The formation of a cooling-induced mesovortex in the trailing stratiform region of a midlatitude squall line. *Mon. Wea. Rev.*, **120**, 2763–2785.

Zhang, D.-L., and R. A. Anthes, 1982: A high-resolution model of the planetary boundary layer–Sensitivity tests and comparisons with SESAME-79 data. *J. Appl. Meteor.*, **21**, 1594–1609.

Zhang, D.-L., and J. M. Fritsch, 1987: Numerical simulation of the meso- β scale structure and evolution of the 1977 Johnstown flood. Part II: Inertially stable warm-core vortex and the mesoscale convective complex. *J. Atmos. Sci.*, **44**, 2693–2612.

Zheng, Y., Q. Xu, and D. J. Stensrud, 1995: A numerical simulation of the 7 May 1985 mesoscale convective system. *Mon. Wea. Rev.*, **123**, 1781–1799.

Zhou Haiguang, Liu Yanying, and Shi Dingpu, 2003: An Analysis of the "5.24" Heavy Rain in Guangdong. *Journal of Nanjing Institute of Meteorology*, **26**(6), 859–864. (in Chinese)